J Mater Sci (2011) 46:1244–1252
DOI 10.1007/s10853-010-4904-7

Effect of negative bias voltage on mechanical and electrochemical nature in Ti–W–N coatings

J. C. Caicedo · L. Yate · G. Cabrera · W. Aperador · G. Zambrano · P. Prieto

Received: 7 May 2010 / Accepted: 6 September 2010 / Published online: 21 September 2010

Abstract Mechanical and electrochemical surface properties of Si (100) and AISI D3 steel substrates-coated Ti–W–N, deposited by r.f. magnetron sputtering process from a binary (50% Ti, 50% W) target in an Ar/N_2 (90%/10%) mixture, have been studied using nanoindentation, Tafel polarization curves and electrochemical impedance spectroscopy (EIS). The crystallinity of the coatings was analyzed via X-ray diffraction (XRD) and the presence of TiN(111), TiN(200), WN_2(107), and W_2N(220) phases were determined. Depth sensing nanoindentation measurements were used to investigate the elasto-plastic behavior of Ti–W–N coatings. Each group of samples was deposited under the same experimental conditions (power supply, Ar/N_2 gas mixture and substrate temperature), except the d.c. negative bias voltage that varied (0, −50, and −100 V) in order to study its effect on the mechanical and electrochemical properties of AISI D3 steel coated with Ti–W–N coatings. The measurements showed that the hardness and elastic modulus increase from 19 to 30 GPa and from 320 to 390 GPa, respectively, as a function of the increasing negative bias voltage. Coating track and coating-substrate debonding have been observed with atomic force microscopy (Asylum Research MFP-3D®) on the indentation sites. Finally, the corrosion resistance of Ti–W–N coatings in 3.5 wt% NaCl solution was obtained from electrochemical measurements in relation to the increase of the negative bias voltage. The obtained results have shown that at the higher negative bias voltage (−100 V), the steel coated with Ti–W–N coatings presented the lower corrosion resistance. The corrosion resistance of Ti–W–N in 3.5 wt% NaCl solution was studied in relation to the increase of the bias voltage.

J. C. Caicedo (✉) · L. Yate · G. Cabrera · G. Zambrano
Thin Film Group, Universidad del Valle, Cali, Colombia
e-mail: jcesarca@calima.univalle.edu.co

L. Yate
Departament de Física Aplicada i Óptica, Universitat de Barcelona, Martí i Franquès 1, Planta 5ª, 08028 Barcelona, Spain

W. Aperador
Department of Mechanical and Mechatronic Engineering, Universidad Militar Nueva Granada, Bogotá, DC, Colombia

P. Prieto
Center of Excellence for Novel Materials—CENM, Calle 13 #100-00 320-026, Cali, Colombia

Introduction

The PVD method via magnetron sputtering processes has been used for coating cutting tools since the 1980's. Among the processes used for this purpose, magnetron sputtering and its reactive variants have proven to be very successful. One of the ways of accessing the importance of this technique, besides the scientific papers, are the patents which sputtering is preferred to the CVD process due to the contamination that occurs in the later (e.g., [1]). Many studies reported in the literature, where ternary materials such as AlCN [2], YSZ [3], CrAlN [4], TiCN [5], $BiMnO_3$ [6], etc. are synthesized with high stability confirm the advantages of the PVD process. The study of W-based coatings produced by magnetron sputtering has been one of the most active research lines in the hard coatings area. The investigation has been focused both on binary systems, such as W–N and W–C [7–9], as well as on the study of an additional third element to these systems (e.g., [10, 11]). In particular, ternary Ti–W–N thin coatings were developed with the specific aim of improving the oxidation behavior of binary coatings (WN) when they are used as protective

surfaces for cutting tools [12, 13]. Nowadays, several research groups are investigating the effects of the substitution of Si, in similar ternary compounds, by another element of the different periodic table group, e.g., titanium, which can generate the (Ti–W–N) material. Therefore, Ti–W–N coatings are useful for microelectronic applications [14, 15]. Ti–W–N coatings for mechanical applications have been prepared by reactive cathodic arc deposition using Ti/W alloy targets and they have been reported as unusually hard PVD coatings particularity useful in coating tool operations [16]. In the hard coatings is possible increase the hardness when is modify the deposition parameters such as voltage bias, therefore, when coatings with high hardness are applied on industrial devices (e.g., cutting tools) the best response in the mechanical performance may be obtain with coatings that present highest hardness, but the optimal performance of coated industrial devices not only is based on high hardness of the coatings, because the corrosion resistance that can provide the coating under aggressive environments is very important. Recent research has shown that the high voltage bias can harmfully affect the response to corrosion for some coatings [5]. In that sense it is very important to evaluate the mechanical and electrochemical properties, determining the synergism between them. The purpose of this study is to produce and characterize the Ti–W–N coatings growth onto the steel surface via a magnetron co-sputtering method with different applied negative bias voltages in order to study the influence of the incorporation of the third element, especially, on the structural, mechanical, electrochemical properties, and superficial protection that the Ti–W–N coatings to steel surface offers for possible surface applications in processes with aggressive environments (e.g., polymer industry).

Experimental setup

Ti–W–N coatings were grown onto Si (100) and AISI D3 steel substrates by r.f. reactive magnetron sputtering. The composition of AISI D3 steel used in the fabrication of moulds for thermoplastic polymer is showed in Table 1. Ti–W–N coatings were obtained by sputtering of a binary (50% Ti, 50% W) target in an Ar/N_2 (90%/10%) mixture. During the deposition process the d.c. negative bias voltages applied to substrate was varied between (0, −50, and −100 V) fixing the other deposition parameters (power supply, Ar/N_2 gas mixture and substrate temperature), in order to investigate its influence on the mechanical and electrochemical properties of deposited coatings. The deposition chamber was evacuated at less than 10^{-5} mbar before the coatings growth process by means of a turbo-molecular pump backed with a mechanical pump. The working pressure was 6×10^{-3} mbar and the r.f. power applied to the target and deposition temperature was 100 W and 400 °C, respectively. All Ti–W–N coatings were deposited with thickness around 1.2 μm.

Table 1 Composition of the AISI D3 steel (wt%)

C	Si	Mn	Cr
2.00	0.20	0.30	11.50

The coatings were characterized by X-ray diffraction (XRD) using a D8 Advance-Bruker diffractometer with a Cu Kα ($\lambda = 1.5418$ Å) radiation source, The X-ray diffraction instrument has been used in thin film for the textures analysis. The mechanical properties (Hardness and elastic modulus) were studied by using a nanoindentation method using an atomic force microscopy (Asylum Research MFP-3D®) device with a diamond Berkovich tip at variable load, under load, and unload mode with a matrix measurements of 25 points and maximum load of 5 mN. The results were evaluated by the Oliver and Pharr method [17]. The electrochemical study was carried out with a Gamry unit, model PCI-4, that was used for DC and AC measurements, through electrochemical impedance spectroscopy (EIS) and Tafel polarization curve techniques at room temperature (25 °C) in static conditions (without aeration), using a cell with a working electrode of an exposed area (1 cm^2), a reference electrode (Ag/AgCl) and a platinum wire counter-electrode under 3.5% NaCl solution at pH 6.2. The solution was prepared using AR grade NaCl dissolved in distilled water. For Nyquist diagrams, frequency sweeps were conducted in the range of 100 kHz to 0.001 Hz using sinusoidal signal amplitude of 10 mV. Diagrams for Tafel polarization curves were obtained at a sweep speed of 0.5 mV/s in a voltage range from −0.25 to 0.25 V, this voltage range was defined with respect to the open circuit potential (OCP) [5]. Finally, for an analyzed corrosion surface process, the surface morphology was characterized by using an optical microscopy Olympus PME-3 with a 50× objective.

Results and discussion

X-ray diffraction analysis

Figure 1 shows the XRD patterns of deposited Ti–W–N material onto Si (100), at d.c. negative bias voltages of 0, −50, and −100 V, related to a cubic structure. In the sample deposited at 0 V, the strongest peak corresponded to the Ti–N (200) plane of f.c.c structure, indicating a light textured growth along this orientation. When the negative bias voltage is increased from 0 to −100 V the coatings

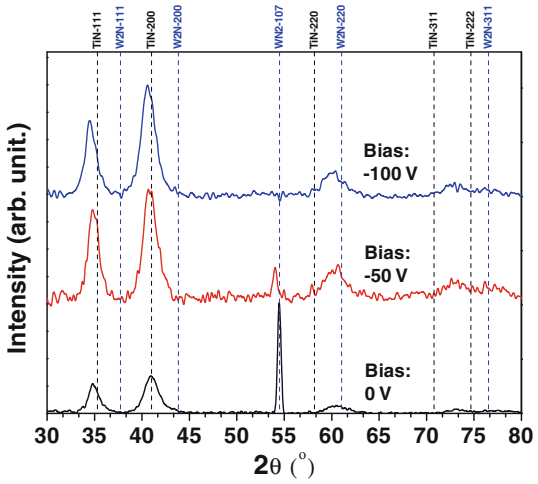

Fig. 1 XRD patterns for Ti–W–N coatings deposited at different bias voltages onto Si (100) substrate. *Dash lines* indicate the position of the peaks obtained from ICDD cards

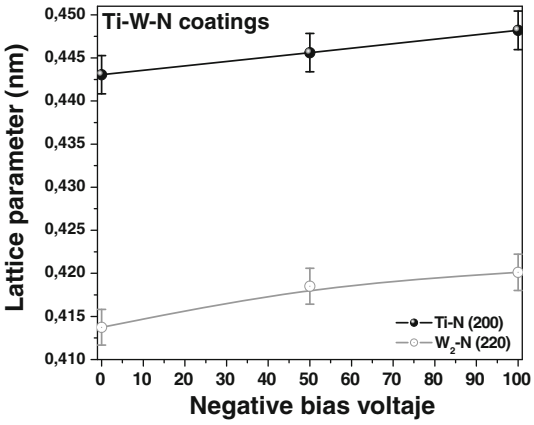

Fig. 2 Lattice parameter for TiN(200) and W_2N(220) within Ti–W–N coatings as function of applied d.c. negative bias voltage (0, −50, and −100 V)

show a high texture growth in the TiN (200) plane. On the other hand, for this patterns it was noted that the W–N_2 (107) phase decreased while the TiN (111), Ti–N (200), and W_2N (220) phases increased when the bias voltage was increased.

For the samples deposited at −50 and −100 V the strongest peaks corresponded to the TiN (200) plane for f.c.c structures. The other weak peaks corresponded to diffractions from the Ti–N (111) and W_2N (220) planes of cubic structures [18]. The possible presence of the Ti–W–N obtained on Si (100) substrate can be associated to a substitution mechanism, where Ti atoms replace W atoms, resulting in a W-ordered Ti–N disordered b.c.c structure in which W and Ti placed at the Wyckoff site 4a, while N atoms randomly occupied the Wyckoff site 4b [10, 19]. This means that the nitrogen gas flow rate directly influences the structure of Ti–W–N coatings. In this study, the nitrogen gas flow rate was around 4 sccm, and when the d.c. negative bias voltage began to increase, the effects induced the facility of the Ti access to the deposition surface; hence, the b.c.c structure is determined by a partially ordered structure with W atoms, creating vacancies in non-metallic sublattice [11, 17, 20]. So, in TiWN coatings, the texture is the distribution of crystallographic orientations of a polycrystalline sample. The crystallographic orientations in TiWN coatings are not random, but have some preferred orientation, thus, the TiWN samples have a weak, moderate or strong texture as function of increasing of negative bias voltage. The degree is dependent on the percentage of crystals having the preferred orientation. Texture is seen in almost all TiWN coatings, and can have a great influence on TiWN mechanicals properties.

Figure 2 shows XRD patterns of 1.2 μm-thick Ti–W–N coatings grown with a d.c. negative bias voltage from 0 to −100 V deposited on Si substrate. TiN and W_2N patterns within Ti–W–N coatings present a FCC type NaCl with high relative intensity corresponds to orientations in the Bragg planes TiN(200) and W_2N(220). From XRD results it is seen that the Ti–W–N coatings are polycrystalline materials but with a little texture at TiN(200) direction, because the (200) direction presents the highest relative intensity. The lattice parameters corresponding with preferential orientation (200) have been determined using the Bragg law written in terms of lattice parameter (a_0):

$$n\lambda = 2\sin(\theta)\cdot\left(\frac{a_0}{\sqrt{h^2+k^2+l^2}}\right) \quad (1)$$

where n is an integer determined by the order given, λ is the wavelength of the X-rays (and moving electrons, protons and neutrons) (1.5406 Å) (hkl) is the reciprocal lattice vector, θ is the angle between the incident ray and the scattering planes, and (a_0) is the lattice parameter [21]. The lattice parameter for Ti–N phase at (200) direction and W_2N phase in (220) direction are shown in Fig. 2. From Fig. 1, the black dash lines correspond to powder diffraction at one preferential orientation for Ti–N and blue dash lines correspond to powder diffraction at one preferential orientation for W_2N according to (00-002-1159 and 00-025-1257 files from ICDD cards, respectively). In Fig. 2, it is observed that the lattice parameter (a_0) for Ti–N and W_2N phases into Ti–W–N coatings decreases as function of applied d.c. negative bias voltage, therefore when the negative bias voltage is increased the Ti–W–N coatings suffers an compressive stress due to ions impact from Ar^+.

Surface analysis of Ti–N–W coatings via AFM

Figure 3 shows a 5 μm × 5 μm image for 1.2 μm-thick Ti–W–N coatings deposited at a d.c. negative bias voltage of −50 V. The general trend in these systems was a

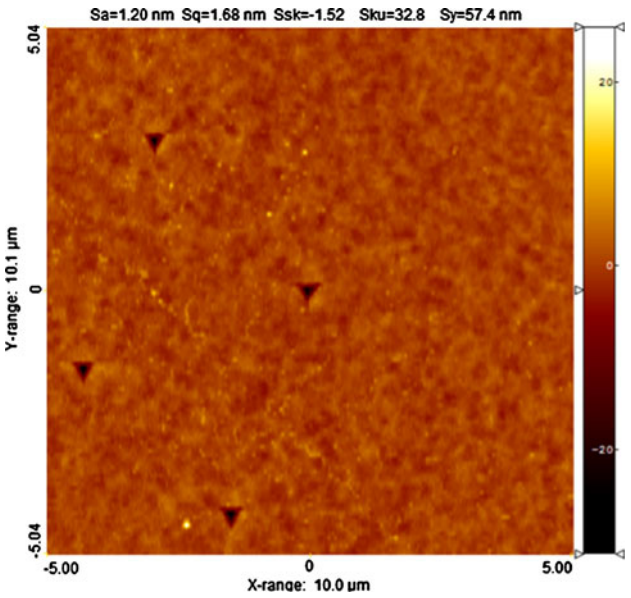

Fig. 3 AFM images for 1.2 µm-thick Ti–W–N coatings grown onto AISI D3 steel substrate with negative bias voltage of −50 V

decrease of the grain size and roughness when the applied bias voltage is increased. Figure 3 also shows the pyramidal traces generated on Ti–W–N surface coatings by the indentation method.

Figure 3 shows the quantitative data extracted from the AFM images. Each data point in the plots represents an average over 3 AFM images. The corresponding error bar was obtained by a standard deviation of the values.

From the Fig. 4 it is possible to compare the grain size and roughness values for the Ti–W–N coatings, therefore, in this article it was observed that a decreasing tendency in both measurements when the d.c. negative bias voltage was increased. The lower grain size value obtained in this study by the Ti–W–N coatings deposited at −100 V (Fig. 4b), represented a decrease at 42%, compared to that obtained for the Ti–W–N coatings deposited at 0 V. This fact is relevant since the continuity of the surface is important for manufacturing tools and mechanics devices under wear and environmental corrosion [22]. The variation of grain size and roughness (Fig. 4a) obtained in the Ti–W–N coatings suggests that Ar^+ ion bombardment generated by the application of negative bias voltages on surface substrates modifies the superficial morphology increasing the energy associated with atoms on the substrate surface and/or the growing coating surface which produce a relative reduction of grain size. On the other hands, many authors reported a correlation between AFM and XRD results, because the AFM analysis delivers surface information (with lateral resolution), but XRD collects information from the space around the normal vector on the surface (from a cross-section); and if this is taken into account it is possible to consider that PVD coating columns can grow "vertically" from the substrate to the "top" and can change their cross-section when the negative bias is modified.

Mechanical properties

It was found that the hardness and elastic modulus of the coatings depended strongly on the applied negative bias voltage. Figure 5a shows the indentation load as a function of the displacement for the Ti–W–N coatings with thickness around 1.2 µm. In Fig. 5, it is possible to observe that the percentage of elastic recovery depends on the applied bias voltage; showing that the sample with the maximum negative bias voltage presents the lower percentage of elastic recovery, R, the greater reduced elastic modulus (390 GPa), and proportional to the higher hardness (30 GPa) [23, 24], Fig. 5b. The increase of hardness can be attributed to the morphological evolution due to the continuous bombardment from energetic Ar^+-ions or neutral atoms and molecules, which serves to peen flatten and compress the coatings close to the density of bulk material by high applied energy on the surface material when the

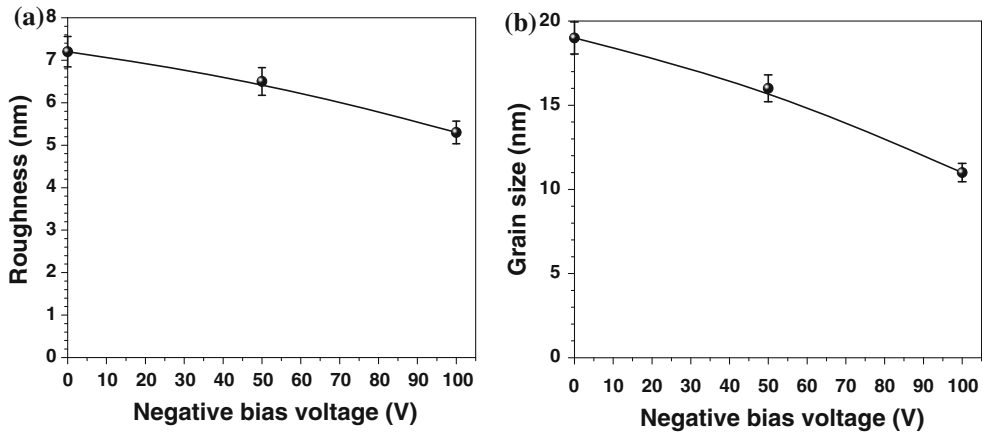

Fig. 4 Correlation between d.c. negative bias voltage with **a** roughness, **b** grain size

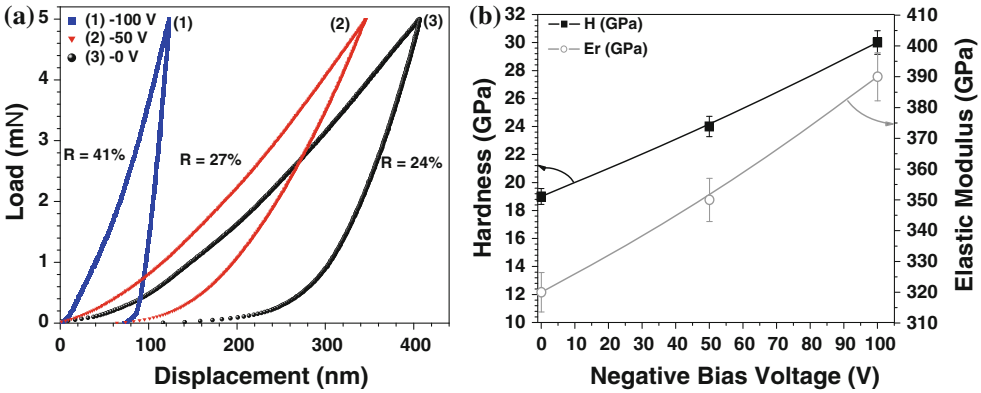

Fig. 5 Mechanical properties of Ti–W–N coatings with thickness around 1.2 μm: **a** Load–displacement curves with an indentation load of 5 mN, **b** Hardness and reduced elastic modulus of deposited coatings measured as a function of negative bias voltages

bias voltage is increased [11, 20]. Moreover, the surface morphology (roughness and grain size) is highly affected by the applied negative bias voltages such as was shown by AFM results. Also, the continuous bombardment from energetic Ar^+-ions or neutral atoms can induce changes in the preferential crystal orientation from W–N_2 (107) to Ti–N (200) which was shown in the XRD results. Therefore, the high hardness measured for Ti–W–N coatings deposited at −100 V is probably due to the increase in the density of coatings, reduction of grain size, reduction of lattice parameter for TiN(200) and W_2N(220) phases into Ti–W–N coatings caused by the ionic bombardment and the increase of the intensity at TiN (200) and W_2N(220) peaks. Consequently, this enhance in mechanical properties as the bias voltage is increase, producing a blockage to the displacement for the cracks, increasing the energy necessary for move that cracks through the coating [20]. Therefore, the increase of applied bias voltage produces an improvement of the mechanical properties of deposited Ti–W–N.

Furthermore, it was observed a dependence of the elasticity with the bias voltage; the higher negative bias voltage corresponds to the higher elastic modulus. Therefore, is possible conclude that the elasticity and elastic recovery (R) of the coatings are improved by increasing the bias voltage. Therefore, from the nanoindentation measurement it was obtained the typical values of elasticity modulus, E_r, and hardness, H, by using the Oliver and Pharr's method [17]. Thus, the elastic recovery for all Ti–W–N coatings was calculated by using the following equation:

$$R = \frac{\delta_{\max} - \delta_p}{\delta_{\max}} \quad (2)$$

where $\delta_{\max}$ is the maximum displacement and δ_p is the residual or plastic displacement, respectively [21, 25]. The equation data was taken from the load–penetration depth curves of indentations for each coating according to Fig. 6a.

In another way according with Kim et al. [26] there is a relationship between elasticity modulus and hardness named plastic deformation resistance (H^3/E^2 ratio), this relation was calculated for all layers in function of the negative d.c. bias voltages and showed in Fig. 6b.

Figure 6b shows a considerable increase in the resistance to the plastic deformation as a function of the increasing of the negative d.c. bias voltages, this fact is due to the hardness and the elasticity modulus also increasing as the bias voltages increased for all coatings. This enhancement in plastic deformation resistance occurs through energetic Ar^+ ion bombardment that increase the lattice parameter, producing the crystallite refinement, point defect formations and the increase of tensile internal stress which improving the hardness of the Ti–W–N coatings.

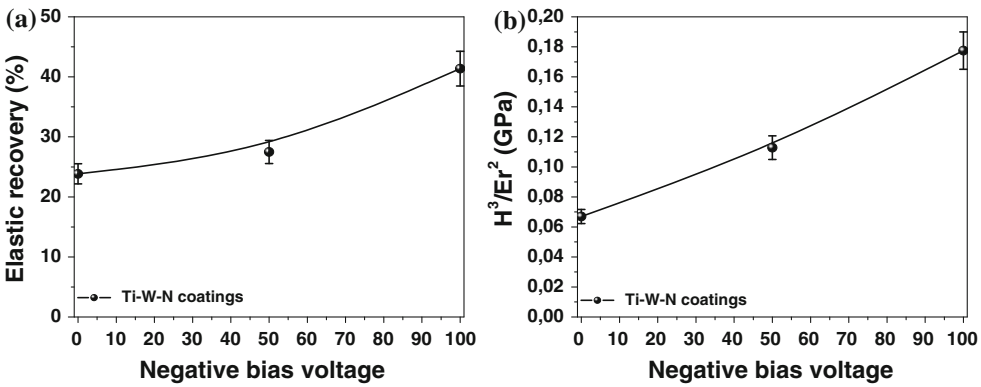

Fig. 6 Elasto-plastic properties with plastic deformation for Ti–W–N coatings deposited with bias voltages from 0 to −100 V: **a** elastic recovery, R, and **b** plastic deformation

From Fig. 6, it is possible to observe the increase in the elastic recovery and plastic deformation resistance with respect to the Ti–W–N single layer coating deposited with 0 V bias voltage. The maximum value was reached for the coating deposited with −100 V, i.e., the plastic deformation due to the applied load is more markedly reduced than that of other single layer coatings with lower applied bias voltage. This effect is clearly correlated to the reduction of grain size, lattice parameter, increasing film density, hardness, and elastic recovery [21].

Electrochemical impedance spectroscopy (EIS) and Tafel polarization curves

Figure 7a shows the Nyquist diagram, an imaginary part of the impedance versus its real part, for the 1.2 μm-thick Ti–W–N coatings grown at different bias voltages: 0 V (filled squared symbol), −50 V (full circles), −100 V (open circles), and for the uncoated AISI D3 steel substrate (filled stars). To simulate the interface coating phenomenon, the *Randles* cell circuit (Fig. 8) was used [27]. In the *Randles* cell circuit the substrate-coating and coating-electrolyte interfaces act as a double layer capacitance in parallel to the coating resistance and the electrolyte resistance due to the ion reaction transfer [27]. A strong dependency of the Nyquist diagrams with the d.c. negative bias voltage was observed. In this study, it has been found that the polarization resistance (R_p) values, obtained from the Nyquist plots, decrease when bias voltages are increased. From the Nyquist diagrams and the equivalent circuit, values were extracted for the polarization resistance (Table 2). It was found that the polarization resistance values decreases when the bias voltage increases. Tafel polarization curves for 1.2 μm-thick Ti–W–N coatings shown in Fig. 7b, were used to calculate the corrosion rate (Table 2). These curves allow findings of the values of anodic and cathodic slopes, which are required to calculate an accurate value of corrosion rate for each of the studied cases. Tafel polarization curves are strongly dependent on the bias voltage, indicating the influence of the growth parameters, in this case the bias voltage, on the corrosion properties of the samples. In the present work it has been found that for AISI D3 steel substrate coated with the Ti–W–N coatings deposited at different bias voltages, the Tafel polarization curves exhibit a shift to the right and toward the top of the graph with respect to the uncovered steel substrate, which indicates a more protective corrosion potential. In addition, it is possible to observe that steel substrates coated with Ti–W–N coatings grown under bias of −100 V, present a left shift, indicating a higher susceptibility to corrosion in the solution compared to the Ti–W–N sample deposited at a bias of 0 V. This behavior is probably due to the porosity and formation of holes or cavities in the coating produced by ion bombardment at higher bias voltages, although Ar-ions produce a reduction of grain size and increase the film density, these bombardments can generate high residual stress which also produces cracks and pores, these defects act as free path and connect the electrolyte with the AISI D3 steel substrate accelerating the corrosive damage [5].

The increase of cracks and pores facilitate the corrosion processes because the more specific superficial area is in contact with the corrosion solution. The values of the corrosion rate calculated from Tafel polarization curves, shown in Table 2, confirms this analysis.

Optical microscopy analysis of Ti–W–N corrosion surface process

Figure 9 shows the optical microscopy images of the surface degradation processes produced by NaCl solution

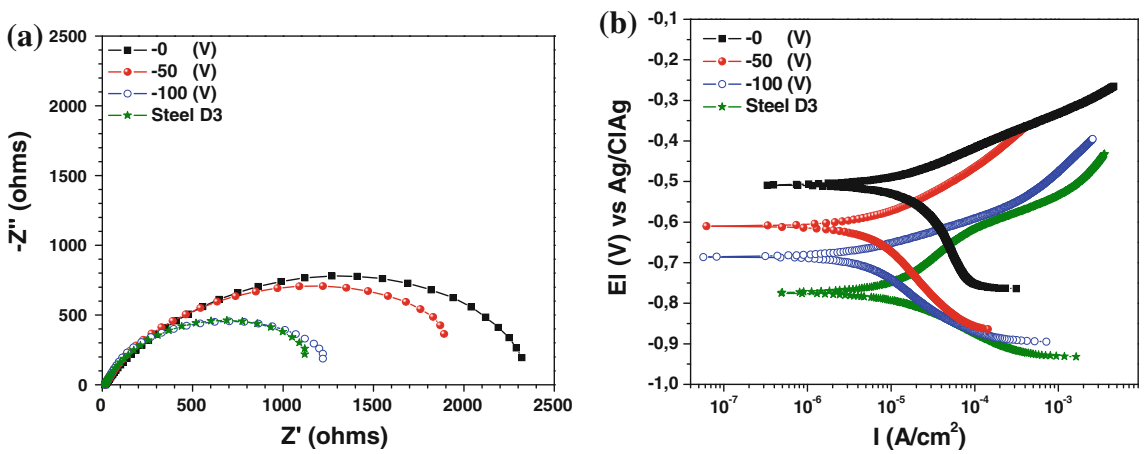

Fig. 7 Ti–W–N coatings with thickness around 1.2 μm grown on the AISI D3 steel substrate at different bias voltages **a** Nyquist plots, **b** Tafel curves

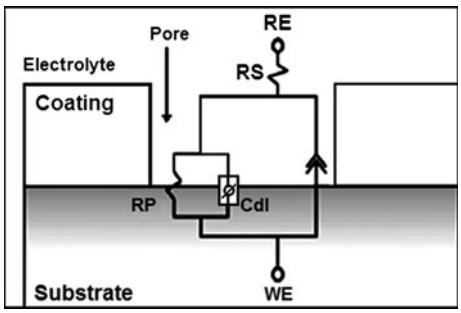

Fig. 8 An equivalent circuit used for simulation of the experimental data, reference electrode (RE), electrolyte resistance (RS), polarization resistance of film (RP), film capacitance (Cdl), working electrode (WE)

attack in Ti–W–N coatings deposited onto steel substrates and uncoated industrial AISI D3 steel substrate. Images were taken under identical conditions of amplification and illumination. Figure 9a clearly shows a superficial attack on uncoated steel substrate, where the superficial general damage is observed. Figure 9b, c shows a partial delamination of coating, due to the corrosion processes, and a surface with few attacks on steel substrate coated with Ti–W–N (−100 and −50 V), respectively. In contrast, in Fig. 9d a surface without considerable attack on steel substrate coated with Ti–W–N (0 V) is observed, due to the excellent corrosion protection presented for this coating, indicating that the ternary coating grown on steel substrate under zero bias voltage is the most resistant to corrosion processes.

On the other hand, with the aim of corroborating the observed by optical images, calculated was a porosity factor associated to the different coatings in agreement with W. Tato and coworkers [28], porosity factor corresponds to the ratio between polarization resistance of the uncoated substrate and the coated substrate as showed in the next equation:

$$P = \frac{R_{p,u}}{R_{p,r-u}} \tag{3}$$

where P is the total coating porosity, $R_{p,u}$ is the polarization resistance of the substrate uncoated, and $R_{p,r-u}$ is the measured polarization resistance of the coating-substrate system. In Fig. 10 the porosity factor values obtained are presented, replacing the electrochemical values on the

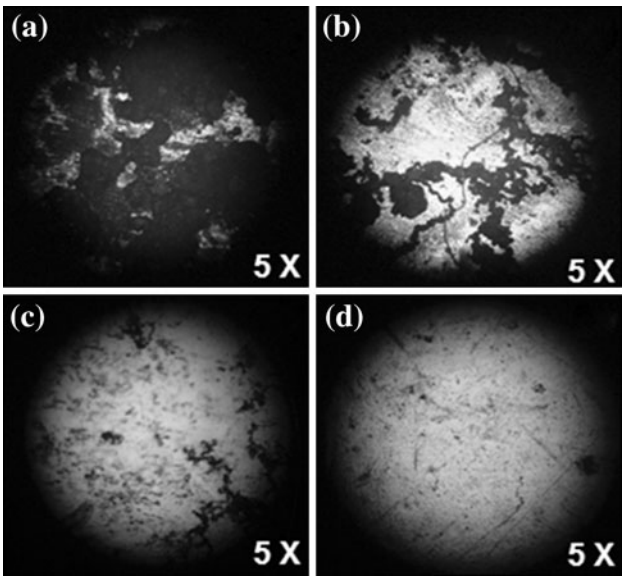

Fig. 9 Optical microscopy images showing the degradation processes of **a** uncoated steel and steel substrate coated with Ti–W–N deposited at **b** −100 V, **c** −50 V, and **d** 0 V

Eq. 3 for all coatings. The analysis of porosity factor values applied in all coatings suggests that the porosity factor increased with the increase of d.c. negative bias voltage and moreover, these results are in agreement with the images from optical microscopy in Fig. 9. Therefore, the polarization resistance values used in the Eq. 3 corresponds to the values extracted from the Nyquist diagrams, specifically, they were extracted from the equivalent circuits determined in each case. As we know from different studies reported in the literature [29, 30], the coatings deposited by PVD techniques are stressed and have defects (e.g., pores and cracks). In that sense, it has assumed that the contact between the electrolyte and the steel substrate take place only through the pores in the coating, the later for made the analysis simple. Therefore, with the Eq. 3 we are only evaluating the effect of the coating in the increasing of the polarization resistance for the steel. If the value of the porosity factor is close to zero (0%) indicates that the coating acts as an inert barrier against the corrosive solution, on the other hand, if the porosity factor is close to unity (100%) indicates that the coating does not act as a barrier for the diffusion of Cl^- corrosive ions and this behavior is attributed to the coating porosity.

Table 2 Polarization resistance values (kΩ cm^2) for Ti–W–N coatings

	Steel D3	Bias 0 V	Bias −50 V	Bias −100 V
Polarization resistance (KΩ cm^2)	1.118	2.325	1.886	1.223
Corrosion rate (mpy)	8.986	2.812	3.756	6.962

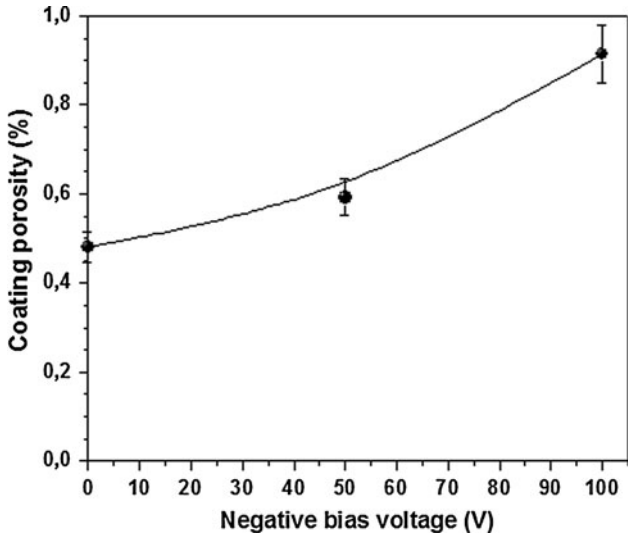

Fig. 10 Coating porosity as function of applied d.c. negative bias voltage

Correlation between mechanical and electrochemical properties

Figure 11 shows the relationship between negative bias voltages, hardness and polarization resistance for Ti–W–N coatings with thickness around 1.2 μm. In Fig. 11 it is clearly shown that the improvement in hardness with an increase in d.c. negative bias voltage by reduction on grain size and changes in crystal orientation within the crystal structure of these materials deposited as hard coatings. The polarization resistance is reduced when the negative bias voltage is increased due to induced porosity by increasing of residual stress which is produced with high applied voltage. It is possible to determine one merit index that

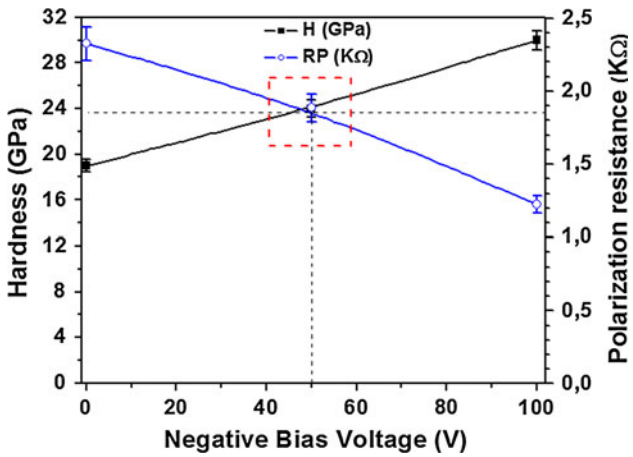

Fig. 11 Correlation between mechanical and electrochemical properties with applied d.c. negative bias voltage

associates the acceptable hardness and polarization resistance with the same d.c. negative bias voltage. Therefore, the Ti–W–N coatings deposited at −50 V offer the best synergy for mechanical and electrochemical properties with good hardness and acceptable polarization resistance.

Conclusion

AISI D3 steel substrates coated with material from a ternary equilibrium diagram Ti–W–N with thickness around 1.2 μm were carried out by reactive r.f. magnetron sputtering by using sputtering process of Ti and W binary target in $N_2 + Ar$ gas mixture at different d.c. negative bias voltages. The present study showed that when the bias voltage is increased the continuous bombardment from energetic Ar^+-ions or neutral atoms can induce changes in the preferential crystal orientation from W–N_2 (107) to Ti–N (200). This effect produced an increase of hardness and elastic modulus of the Ti–W–N, where the ion bombardment serves to peen flatten and compress the coatings close to the density of bulk material by high applied energy on the surface material when the bias voltage is increased which produces lower gain size. The higher hardness and reduced elastic modulus were found at the higher negative bias voltage (−100 V), with an increase of approximately 61 and 22%, respectively, with respect to the Ti–W–N deposited at 0 bias voltage. Furthermore, the increase in the elastic recovery resistance and plastic deformation with respect to the Ti–W–N single layer coating deposited with 0 V bias voltage. The maximum value was reached for the coating deposited with −100 V, therefore it was observe an increase at the plastic deformation resistance and elastic recovery around 42 and 59%, respectively.

Conversely, the effect of the increase of the bias voltage on the morphology of surface and electrochemical behavior of Ti–W–N ternary nitrides coatings was the opposite. The results of the electrochemical and optical microscopy analysis, indicated that an increase of bias voltage produced a partial delamination of coatings and decrease the polarization resistance, especially at bias voltages of −100 V and therefore, it allowed the penetration of the of Cl^- of the electrolyte toward the steel surface. However, the passivation of Ti–W–N coatings generate a protective layer creating better resistance to corrosive events than uncoated industrial AISI D3 steel substrate.

The merit index found in this study suggests that Ti–W–N coatings deposited at a bias of −50 V offer the best synergy for mechanical and electrochemical properties.

Acknowledgements This work was supported by COLCIENCIAS and by the Excellence Center for Novel Materials, CENM, under the RC-043-2005 contract with Colciencias.

References

1. Rich P, Burgess R, O'Sullivan J, Rimmer N (2004) US2004214417
2. Yate L, Caicedo JC, Hurtado Macias A, Espinoza-Beltrán FJ, Zambrano G, Muñoz-Saldaña J, Prieto P (2009) Surf Coat Technol 203:904
3. Amaya C, Aperador W, Caicedo JC, Espinoza-Beltrán FJ, Muñoz-Saldaña J, Zambrano G, Prieto P (2009) Corros Sci 51:2994
4. Sanchéz JE, Sanchéz OM, Ipaz L, Aperador W, Caicedo JC, Amaya C, Hernández Landaverde MA, Espinoza Beltran F, Muñoz-Saldaña J, Zambrano G (2010) Appl Surf Sci 256:2380
5. Caicedo JC, Amaya C, Yate L, Aperador W, Zambrano G, Gómez ME, Alvarado-Rivera J, Muñoz-Saldaña J, Prieto P (2010) Appl Surf Sci 256:2876
6. Grizalez M, Martínez E, Caicedo JC, Heiras J, Prieto P (2008) Microelectron J 39:1308
7. Castanho JM, Vieira MT (1998) Surf Coat Technol 102:50
8. Zambrano G, Prieto P, Perez F, Rincon C, Galindo H, Cota-Araiza L, Esteve J, Martinez E (1998) Surf Coat Technol 108–109:323
9. Rincon C, Zambrano G, Carvajal A, Prieto P, Galindo H, Martínez E, Lousa A, Esteve J (2001) Surf Coat Technol 148:277
10. Louro C, Cavaleiro A (1999) Surf Coat Technol 116–119:74
11. Cavaleiro A, Trindade B, Vieira MT (2003) Surf Coat Technol 174–175:68
12. Marques AP, Cavaleiro A (2003) Thin Solid Films 441:150
13. Piedade AP, Gomes MJ, Pierson JF, Cavaleiro A (2006) Surf Coat Technol 200:6303
14. Moser JH, Tian F, Haller O, Bergstrom DB, Petrov I, Green JE, Wiemer C (1994) Thin Solid Films 253:445
15. Oparowski JM, Quaranta DF, Biederman RR, Sisson, Jr, RD (1988) Microstruct Sci 16:379
16. Hurkmans T, Trinh T, Lewis DB, Brooks JS, Munz W-D (1995) Surf Coat Technol 76–77:159
17. Oliver WC, Pharr GM (1992) J Mater Res 7(6):1564
18. Shaginyan LR, Misina M, Zemek J, Musil J, Regent F, Britun VF (2002) Thin Solid Films 408:136
19. Silva PN, Dias JP, Cavaleiro A (2005) Surf Coat Technol 200:186
20. Anderson PM, Li C (1995) Nanostruct Mater 5(3):349
21. Caicedo JC, Amaya C, Yate L, Zambrano G, Gómez ME, Alvarado-Rivera J, Muñoz-Saldaña J, Prieto P (2010) Appl Surf Sci 256:5898
22. Brett CMA, Cavaleiro A (1998) Thin Solid Films 322:263
23. Navabpour P, Teer DG, Hitt DJ, Gilbert M (2006) Surf Coat Technol 201:3802
24. Keller G, Barzen I, Erz R (1991) Fresen J Anal Chem 341:349
25. Hajek V, Rusnak K, Vlcek J, Martinu L, Hawthorne HM (1997) Wear 213:80
26. Kim GS, Lee SY, Hahn JH (2003) Surf Coat Technol 171:91
27. Randles JEB (1947) Discuss Faraday Soc 1:11
28. Tato W, Landolt D (1998) J Electrochem Soc 145:4173
29. Chang K-L, Chung S-C, Lai S-H, Shih H-C (2004) Appl Surf Sci 236:406
30. Altun H, Sen S (2005) Surf Coat Technol 197:193